Non-instanton tunneling: Semiclassical and quantum interpretations

Kin'ya Takahashi
The Physics Laboratories, Kyushu Institute of Technology, Kawazu 680-4, Iizuka 820-8502, Japan

Kensuke S. Ikeda
Department of Physics, Ritsumeikan University, Noji-higashi 1-1-1, Kusatsu 525-8577, Japan
(Received 8 March 2011; published 11 August 2011)

Tunneling essentially different from instanton-type tunneling, say noninstanton tunneling, is studied from both semiclassical and quantum viewpoints. Taking a periodically perturbed rounded-off step potential for which the instanton-type tunneling is substantially prohibited, we analyze change of the tunneling probability with change of the perturbation frequency based on the stable-unstable manifold-guided tunneling (SUMGT) theory, which we have recently introduced. In the large and small limits of the frequency, the tunneling rate rapidly decays, but it is markedly enhanced in an intermediate range. We will also make a quantum interpretation of the noninstanton tunneling by using an exactly solvable model—a periodically perturbed right-angled step potential. Analysis with this model shows that SUMGT is considered as a sort of photoassisted tunneling through a large energy gap induced with absorbing a huge number quanta, which is completely different from the instanton-type tunneling. Both approaches from the semiclassical and quantum viewpoints complement each other to cause a better understanding of noninstanton tunneling.

DOI: 10.1103/PhysRevE.84.026203 PACS number(s): 05.45.Mt, 03.65.Xp, 03.65.Sq

I. INTRODUCTION

In last two decades, crucial developments in understanding tunneling in multidimensional systems have been achieved. Various novel tunneling phenomena, e.g., chaos-assisted tunneling and resonance-assisted tunneling, have been predicted, found, and observed theoretically, numerically, and experimentally [1–10]. The basic mechanisms of those tunneling phenomena have been interpreted in various ways from semiclassical and quantum points of view and further from hybrid views. For example, resonance-assisted tunneling was first predicted with a hybrid method of classical, semiclassical, and quantum dynamics to understand an enhanced tunneling rate in the presence of classical resonances, which is unexplainable by the simple fictitious integrable model [9], and it was further improved in various ways and applied to several different situations [10]. Furthermore, it is probably possible for its mechanism to be explained with the very rigorous (complex) semiclassical method introduced by Shudo *et al.*—Julia-set assisted tunneling [11,12]. It is considered that those methods complement each other to comprehend all aspects of resonance-assisted tunneling.

Most studies on multidimensional tunneling have been done for discrete time systems, i.e., mapping or kicked rotor, rather than continuous time systems [1–3], because it is easier to handle discrete time systems than continuous time systems, especially in the treatment of the complex semiclassical method [11,12]. However, to make a comparison between novel tunneling phenomena in multidimensional systems and instanton-type tunneling in classically integrable or nearly integrable systems [13] one needs to study continuous time systems [6,7,14–18]. This is because the study of instanton tunneling created with imaginary time evolution requires analytical continuation of the system under consideration to a complex time domain [13,19], but the discrete time systems have no analytical continuation to complex time, namely, δ kick as a distribution is not an analytical function and has no analytical extension to the complex plane.

In recent works we have found a novel tunneling phenomenon different from the instanton-type tunneling for multidimensional barrier systems and have provided its semiclassical interpretation [14,15]. The presence of the same semiclassical mechanism was later reconfirmed in Ref. [18] in a slightly different situation. In this semiclassical mechanism, trajectories contributing to tunneling are guided by complex stable and unstable manifolds of the saddle orbit above the top of a potential barrier, for brevity called SUMGT (stable-unstable manifold guided tunneling). SUMGT is essentially the same as the Julia-set assisted tunneling introduced by Shudo *et al.*, in which forward and backward Julia sets, almost equivalent to complex stable and unstable manifolds [20,21], guide tunneling trajectories even in the case that chaos exists in the real space [11,12], although they have treated tunneling in discrete systems.

In multidimensional barrier tunneling, two types of tunneling mechanisms coexist, instanton-type tunneling and SUMGT, and which tunneling mechanism dominates the tunneling process is determined by the competition between them [16,17]. Actually one that is nearer in the imaginary depth of contributing tunneling trajectories to the real plane than the other is the winner of the competition. The dominant tunneling mechanism, i.e., the winner of the competition, changes places with the other with changes of parameters. The drastic change is observed with change of the perturbation frequency [17]. In the low-frequency limit, the adiabatic approximation based on the instanton, i.e., the time average of the instanton over the perturbation period, works well, which is also expected from some other works [22]. In a mid-frequency range, which is the inherently multidimensional regime, SUMGT governs the tunneling process instead of the instanton. In the high-frequency limit, tunneling converges to that of the unperturbed system, i.e., the unperturbed instanton.

In this paper we focus on the tunneling caused by SUMGT and investigate the change of the tunneling probability with the change of the perturbation frequency. To extract the tunneling caused by SUMGT, we adopt as a model system a periodically perturbed rounded-off step potential, which was introduced in our recent paper [23]. For the step-shaped potential extending over the semi-infinite space, the instanton-type tunneling is substantially prohibited. Indeed, if the energy of an input particle is taken small enough, the instanton tunneling tail decreases in the potential wall exponentially and becomes infinitesimally small only at a small distance from the potential edge.

Even for that case, if the perturbation is turned on, SUMGT starts to work and extremely enhances the tunneling rate in a middle range of perturbation frequency [23]. Only the noninstanton tunneling caused by SUMGT is observed for this case, and it is a good model to investigate characteristics of the purely distilled SUMGT. In this paper we explore the change of tunneling probability through the whole frequency range from a semiclassical viewpoint and evaluate in detail the asymptotic decay rates in low-frequency and high-frequency limit, in which the tunneling rate is expected to decay due to the lack of instanton-type tunneling. In the low-frequency limit, the imaginary depth of SUMGT trajectories increases, giving rise to a very rapid decrease in the tunneling rate. On the other hand, at too high frequencies the particle has little chance of gaining a piece of energy strong enough to induce noninstanton tunneling, so that the tunneling rate decays exponentially.

We also make a quantum interpretation of the noninstanton tunneling caused by SUMGT by using an exactly solvable model, a periodically perturbed right-angled step potential, although a complex semiclassical method cannot be applied to this model due to its nonanalytical nature. For this model, tunneling phenomena similar to those caused by SUMGT are observed. Analysis of the tunneling by using this model clarifies the meaning of SUMGT and the difference between SUMGT and the instanton-type tunneling from a quantum dynamics point of view. Actually SUMGT, especially in a low-frequency range, is interpreted as a sort of photoassisted tunneling through a large energy gap induced with absorbing a huge number quanta. Both approaches, from the semiclassical and quantum viewpoints, complement each other and seem to be necessary in order for a better understanding of noninstanton tunneling and furthermore, tunneling in multidimensional systems.

II. MODEL SYSTEM AND QUANTUM RESULTS

As a model system for which the instanton-type tunneling is substantially prohibited, we have introduced a periodically perturbed rounded-off step potential in recent work [23]. In this paper we use the same model system, whose Hamiltonian is given by

$$\hat{H}(Q,P,\omega t) = \frac{1}{2}\hat{P}^2 + (1+\epsilon\sin\omega t)\frac{1}{1+\exp Q}. \qquad (1)$$

Let us assume that a plane wave is coming from positive infinity in Q with a constant momentum $P_I(<0)$. So, a scattering eigenstate, more precisely, a quasistationary state, is formed and represented with the wave operator [24],

$$\langle Q_O|\hat{\Omega}_1^+(t_O)|P_I\rangle = \lim_{|Q_I|\to\infty}\sqrt{\frac{|P_I|}{2\pi\hbar}}e^{iP_IQ_I/\hbar} \times \int_0^\infty ds\langle Q_O|\hat{U}(\omega t_O\ \omega t_O-\omega s)|Q_I\rangle\exp\left\{\frac{i}{\hbar}E_Is\right\}, \qquad (2)$$

where $\hat{U}$ denotes the propagator of the system,

$$\hat{U}(\theta+\omega t:\theta) = \mathcal{T}\exp\left\{-\frac{i}{\hbar}\int_0^t\hat{H}(\theta+\omega s)\right\}, \qquad (3)$$

and $\mathcal{T}$ indicates the time-ordering operator. The subscripts of dynamical variables I and O indicate input and output, respectively.

The quantum probability observed at $Q=Q_O$ in the transmissive side is caused by tunneling, if the input energy E_I $(=P_I^2/2)$ is taken so small that the corresponding classical particle with any initial phase of the perturbation is kicked back by the oscillating potential. Figure 1 shows scattering eigenstates as a function of Q_O at four different values of ϵ, $\epsilon=0$, 0.05, 0.1, and 0.2. At $\epsilon=0$, i.e., the unperturbed case, the tunneling tail penetrating into the potential wall drops off very quickly, which means that the instanton tunneling is substantially prohibited. However, once the perturbation is applied, the tunneling rate is extremely enhanced and the probability amplitude of each eigenstate does not drop, keeping a nearly constant value over the transmissive region $(Q<0)$, which increases with ϵ. As shown in Ref. [23], the physical origin of such remarkable effects can be explained by SUMGT.

The energy spectrum of the tunneling wave is defined from the wave operator (2) as

$$Sp(E) = \left|\frac{1}{\sqrt{2\pi\hbar}}\int_{-\infty}^{\infty}\langle Q_O|\Omega_1^+(\omega t_O)|P_I\rangle e^{\frac{i}{\hbar}(E-E_I)t_O}dt_O\right|^2. \qquad (4)$$

Figure 2 shows the resultant energy spectra at $\epsilon=0.05$, 0.1, and 0.2. Each spectrum forms a plateau: its height increases

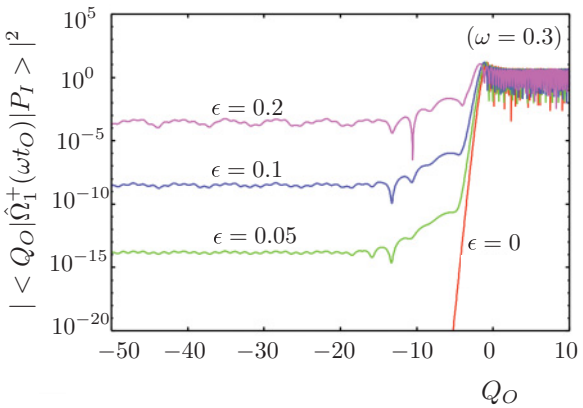

FIG. 1. (Color online) Probabilistic amplitudes of scattering eigenstates for the rounded-off step potential at $\epsilon=0$, 0.05, 0.1, and 0.2. The parameters are chosen as $E_I=0.75$, $\omega=0.3$, and $\hbar=1000/(3\pi\times 2^{10})\sim 0.1036$.

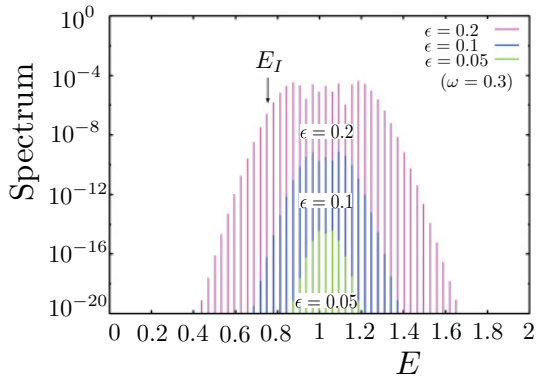

FIG. 2. (Color online) Tunneling energy spectra calculated by Eq. (4) at $\epsilon = 0.05$, 0.1, and 0.2.

with ϵ and its flat top has a width nearly equal to 2ϵ. Such a plateau-shaped tunneling spectrum is the fingerprint of SUMGT [15].

III. SEMICLASSICAL WAVE OPERATOR

The semiclassical expression of the wave operator is given by [24]

$$\langle Q_O|\hat{\Omega}_1^+(t_O)|P_I\rangle \sim \sum_{\text{c.t.}} \lim_{Q_I\to\infty} \sqrt{\frac{|P_I|}{2\pi\hbar}} e^{iP_IQ_I/\hbar} \times \left[\frac{1}{P_I}\frac{\partial^2 S_\Omega}{\partial E_I \partial Q_O}\right]^{1/2} \exp\left\{\frac{i}{\hbar} S_\Omega(Q_O,t_O,Q_I,E_I)\right\}, \quad (5)$$

where $S_\Omega(Q_O,t_O,Q_I,E_I)$ denotes the classical action integral defined by

$$S_\Omega(Q_O,t_O,Q_I,E_I) \equiv \int_{Q_I}^{Q_O} P\,dQ - \int_{t_I}^{t_O} H(Q,P,\omega t)\,dt + E_I[t_O - t_I(Q_O,t_O,Q_I,E_I)]. \quad (6)$$

The summation in Eq. (5), i.e., $\sum_{\text{c.t.}}$, is taken over all contributing trajectories, which satisfies the input and output boundary conditions simultaneously.

Let us consider the boundary condition. The dynamical variables, which are independent variables of the classical action $S_\Omega(Q_O,t_O,Q_I,E_I)$, become quantum observables; then Q_I and E_I at input, and Q_O and t_O at output must take fixed real values. On the other hand, the initial time t_I is canonically conjugate to E_I and cannot be observed quantum mechanically. According to Miller's prescription for the semiclassical method, which is necessary to treat tunneling problems [19], any complex number can be assigned to a quantum mechanically unobserved variable. So t_I takes an arbitrary complex number. Then to find the trajectories satisfying the input and output boundary conditions, the initial time t_I can be used as a complex search parameter on the initial plane $\mathcal{I}$:

$$\mathcal{I} \equiv \{Q,P,t_I|Q = Q_I,\ P = P_I, t_I \in \mathbf{C}\}. \quad (7)$$

To reproduce the scattering eigenstate as a function of Q, Q_O is moved along the real axis, i.e., $Q_O \in \mathbf{R}$, with a fixed t_O. So the search parameter t_I moves along certain curves on the complex plane called complex branches. This set of the complex branches is given by [11,14,24]

$$\mathcal{M} = \{t_I|\text{Im}Q(t_O - t_I,t_I,P_I,Q_I) = 0\}. \quad (8)$$

The set of trajectories starting from $t_I \in \mathcal{M}$ forms a Lagrange manifold at $t = t_O$,

$$\mathcal{L} = \{Q,P|Q(t_O - t_I,t_I,P_I,Q_I), P(t_O - t_I,t_I,P_I,Q_I), t_I \in \mathcal{M}\}, \quad (9)$$

and contributes to reproducing the scattering eigenstate. We are interested in the complex trajectories starting from the $\mathcal{M}$ set and reaching a classically forbidden region, namely, tunneling trajectories.

IV. CLASSICAL SOLUTION OF THE UNPERTURBED SYSTEM

In this section we introduce the classical solution of the unperturbed system and discuss the location change of its singularities on the complex time plane, depending on the energy. The solution for $0 < E < 1$ is given as an implicit form:

$$t - t_0 = \frac{1}{\sqrt{2E}}\log(4EY - 2 - 4\sqrt{E^2Y^2 - EY}) + \frac{1}{i}\frac{1}{\sqrt{-k}}\log\left[i\left(-1 + 2E + \frac{k}{(Y-1)}\right) - \frac{\sqrt{-2k(EY^2 - Y)}}{Y-1}\right], \quad (10)$$

where the variable Y is defined by $Y \equiv 1 + \exp Q$, k is given by $k = 2(E-1)$, and t_0 is a time origin of this solution.

The turning point of the real trajectory Q_{turn} is determined by $E = V_0(Q_{\text{turn}}) = 1/Y(Q_{\text{turn}})$, where $V_0(Q) = \frac{1}{1+\exp Q}$, then the time t_{turn} at which it reaches Q_{turn} is given by $t_{\text{turn}} = t_0 + \frac{1}{\sqrt{2E}}\log 2 - \frac{\pi}{2\sqrt{-k}}$. At the turning point $Q = Q_{\text{turn}}$, both square roots in Eq. (10) vanish and it becomes a branch point of the implicit form of the solution. Since the solution (10) gives a trajectory for $t < t_{\text{turn}}$ coming from positive infinity in Q, then the reflective trajectory for $t > t_{\text{turn}}$ and the instanton trajectory from $t = t_{\text{turn}}$ to $t_{\text{turn}} - i\infty$ are obtained by analytical continuation of the solution (10), with a full round and a half round of Y around $Y = 1/E$, respectively.

The singularities of the potential given by $Y = 0$, i.e., $Q_s = i(2n+1)\pi$, correspond, but not one-to-one, to singularities of the explicit form of the solution $Q(t)$. There are an infinite number of singularities, but only four dominant singularities on the first Riemann sheet,

$$t_s - t_{\text{turn}} = \pm i\frac{\pi}{\sqrt{2E}} \pm \frac{\pi}{\sqrt{-k}}, \quad (11)$$

are important for our discussion. Figure 3(a) shows the location of the singularities and two topologically different integration paths. The integration paths C_0 and C_I give reflective and instanton trajectories, respectively.

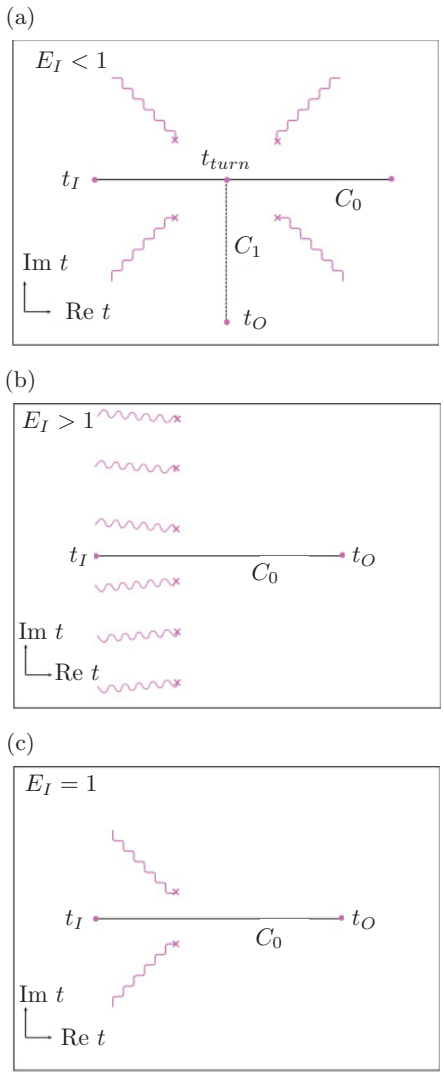

FIG. 3. (Color online) Singularities and integration paths on the complex t plane: (a) $E_I < 1$ and (b) $E_I > 1$, and (c) $E_I = 1$.

The solution (10) also has a branch point at $E = 1$, namely, $k = 0$. The analytical continuation gives an appropriate form of the solution for $E > 1$,

$$t - t_0 = \frac{1}{\sqrt{2E}} \log(4EY - 2 - 4\sqrt{E^2Y^2 - EY}) + \frac{1}{\sqrt{k}} \log\left(-2 + 4E + \frac{2k + 2\sqrt{2k(EY^2 - Y)}}{Y - 1}\right), \tag{12}$$

where t_0 is different from t_0 in Eq. (10) by a certain constant. The dominant singularities of the explicit form $Q(t)$ on the first Riemann sheet are given by

$$t_s - t_0 = \frac{1}{\sqrt{2E}}(\log 2 \pm i\pi) + \frac{1}{\sqrt{k}}(\log 2 + 2\pi mi). \tag{13}$$

They are located along a vertical line as shown in Fig. 3(b), and the location of the singularities is completely different from that of the solution for $0 < E < 1$. The trajectory integrated along the path C_0 reaches negative infinity in Q.

The solution at $E = 1$, i.e., $k = 0$, is given by

$$t - t_0 = \frac{1}{\sqrt{2}} \log(4Y - 2 - 4\sqrt{Y^2 - Y}) + \frac{\sqrt{2(Y^2 - Y)}}{Y - 1}. \tag{14}$$

As shown in Fig. 3(c), there are only two dominant singularities of the explicit form $Q(t)$ on the first Riemann sheet, whose positions are given by

$$t_s - t_0 = \frac{1}{\sqrt{2}}(\log 2 \pm i\pi). \tag{15}$$

This means that the other dominant singularities are diverged to infinity at $k = 0$, which is necessary to induce the location change of singularities, i.e., the topological change of Riemann sheets, between the solutions for $0 < E < 1$ and $E > 1$.

The divergence of a part of singularities of a solution is the remarkable feature of stable and unstable manifolds [14]. Therefore the separatrix given by the solution (14) at $k = 0$ is categorized to the group of those invariant manifolds which possess the same property characterizing stable and unstable manifolds from the view point of complex dynamics.

V. ANALYSIS BASED ON STABLE-UNSTABLE MANIFOLD GUIDED TUNNELING

A. Stable-unstable manifold guided tunneling

As discussed in the previous section, the separatrix at $E = 1$ is the same kind of invariant manifold as the stable and unstable manifolds. Then it is expected that the same type of tunneling as SUMGT occurs when a periodical perturbation is applied to the system, namely, the perturbed separatrix guides tunneling trajectories the same way as the stable manifold does in the multidimensional barrier tunneling.

Figure 4 shows a schematic picture of the Poincaré map of the periodically perturbed rounded-off step-potential system. The separatrices playing the roles of stable and unstable manifolds are indicated by W_s and W_u, respectively. In the case of rounded-off step potential, it may be considered that the unstable periodic orbit moves to negative infinity in Q and the momenta of W_s and W_u asymptotically converge on zero as Q goes to negative infinity. The initial plane in a unit period of the perturbation is indicated by $\mathcal{I}$.

For the situation in which tunneling occurs, Re$\mathcal{I}$ does not touch ReW_s, and mappings of Re$\mathcal{I}$ form an invariant manifold drawn by a thin black curve, which never goes to the product

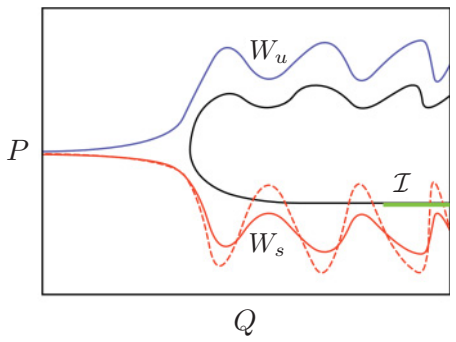

FIG. 4. (Color online) Brief sketch of SUMGT.

side. However, the variation of W_s is usually amplified in the complex domain, as shown by the dashed (red) curve, so that an intersection between W_s and $\mathcal{I}$ occurs in the complex domain forming an isolated point at $t_I = t_{Ic}$, called the critical point [14,15]. The SUMGT trajectories are those trajectories which start from a small neighborhood of the critical point. Some of SUMGT trajectories go to negative infinity in Q guided by the complex W_s, thereby contributing to tunneling. The others are also guided by the complex W_s but take a turn to the opposite direction somewhere on the way and go back to the reflective side along W_u, contributing to reflection.

Therefore, this SUMGT mechanism for the periodically perturbed rounded-off potential is essentially the same as the SUMGT mechanism for multidimensional barrier systems and is completely different from the instanton-type tunneling. For the step potential, an instanton trajectory spends a negative infinite imaginary time to reach negative infinity in Q, thereby gaining an infinite large imaginary action and the tunneling probability induced by instanton substantially becomes zero. Then SUMGT is the only semiclassical mechanism contributing to tunneling for the periodically perturbed rounded-off potential.

B. Melnikov method: Imaginary depth of the critical point

The existence of the critical point can be proved by using the Melnikov method [14,15,25,26]. Actually, the energy of a trajectory on the separatrix W_s can be evaluated by

$$H[Q_s(t),P_s(t),t] = 1 + \epsilon \sin\omega t + \Delta H_M(t), \tag{16}$$

where

$$\Delta H_M(t) = \int_\infty^t \frac{\partial H}{\partial t'} - \epsilon\omega\cos\omega t' dt' = \int_\infty^t (V_0[Q_s(t)] - 1)\epsilon\omega\cos\omega t' dt', \tag{17}$$

and $V_0(Q) \equiv \frac{1}{1+\exp Q}$ is the unperturbed potential. $Q_s(t)$ denotes the trajectory on the separatrix W_s and is replaced by the unperturbed solution (14) for the first-order approximation, namely, the Melnikov method [25,26]. The time origin t_0 in Eq. (14) determines the relative phase with respect to the periodical perturbation, and the initial time t_I at $Q = Q_I$ is given by

$$t_I = t_0 - \frac{Q_I}{\sqrt{2}} + \sqrt{2}. \tag{18}$$

As a result, the input energy for a given t_0 is obtained as

$$\lim_{t_I\to-\infty} H(t_I,t_0) = \epsilon\omega\chi_{\cos}\cos\omega t_0 - \epsilon\omega\chi_{\sin}\sin\omega t_0 + 1 + \epsilon\sin\omega t_0, \tag{19}$$

where $\chi_{\cos}$ and $\chi_{\sin}$ are respectively defined by

$$\chi_{\{\cos\,,\,\sin\}} \equiv \int_\infty^0 (V_0[Q_{s0}(\tau,t_0=0)] - 1)\{\cos\,,\,\sin\}\omega\tau d\tau + \int_0^{-\infty} V_0[Q_{s0}(\tau,t_0=0)]\{\cos\,,\,\sin\}\omega\tau d\tau, \tag{20}$$

where $Q_{s0}(t,t_0)$ denotes the unperturbed solution on W_s with the time origin t_0. Since the energy takes a real value E_I on the initial plane $\mathcal{I}$, then the intersection t_{Ic} between the initial plane $\mathcal{I}$ and the separatrix W_s, namely, t_{0c} through Eq. (18), is given by

$$E_I = 1 + \epsilon A(\omega)\sin(\omega t_{0c} + \phi) \in \mathbf{R}, \tag{21}$$

where

$$\tan\phi = \frac{\omega\chi_{\cos}}{1 - \omega\chi_{\sin}} \tag{22}$$

and

$$A(\omega) = \sqrt{(1-\omega\chi_{\sin})^2 + \omega^2\chi_{\cos}^2}. \tag{23}$$

In the case that the intersection occurs in the complex domain, i.e., $\epsilon A(\omega) < 1 - E_I$, the imaginary depth of the intersection is given by

$$\mathrm{Im}t_{Ic} = \frac{1}{\omega}\cosh^{-1}[(1-E_I)/\epsilon A(\omega)]. \tag{24}$$

Even in the limit of $\omega \to 0$, each $\chi_{\cos\,,\,\sin}$ takes a finite value, so that $A(\omega) \to 1$. Then the imaginary depth of the critical point becomes

$$\mathrm{Im}t_{Ic} \sim \frac{1}{\omega}\cosh^{-1}\left(\frac{1-E_I}{\epsilon}\right) \tag{25}$$

$$\sim \frac{1}{\omega}\log\left(\frac{2(1-E_I)}{\epsilon}\right), \quad (\epsilon \ll 1 - E_I). \tag{26}$$

The approximation used in the most right-hand side (26) is valid only for $\epsilon \ll 1 - E_I$. Figure 5 shows the change of $\mathrm{Im}t_{Ic}$ with ω at $\epsilon = 0.05$, 0.1, and 0.2. In a low-frequency range $\omega < 0.1$, $\mathrm{Im}t_{Ic}$ decreases inversely proportional to ω and also decreases at a fixed ω with ϵ, as indicated by Eq. (25). Further, the approximation (26) works well for $\epsilon = 0.05$ and 0.1, but not for $\epsilon = 0.2$. On the other hand, it seems to converge on $\pi/\sqrt{2}$ in the limit $\omega \to \infty$, regardless of ϵ. The behavior of $\mathrm{Im}t_{Ic}$ with ω is essentially the same as that for the periodically perturbed Eckart potential [17].

C. Tunneling probability estimated with SUMGT

As shown in Ref. [23], the full complex semiclassical calculation with all contributing trajectories starting from the $\mathcal{M}$ set defined by Eq. (8) reproduces every detail of the tunneling part of a scattering eigenstate. However, it is a very huge task. Indeed, in order to do this, summing up

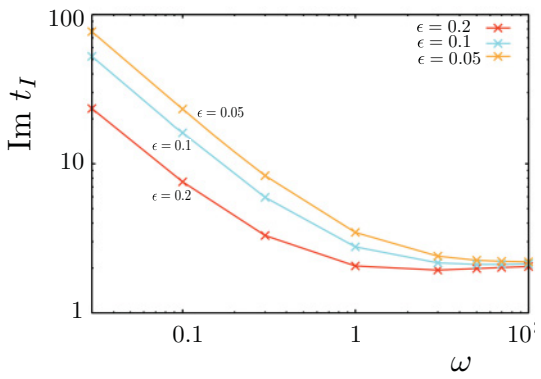

FIG. 5. (Color online) Imaginary depth of the critical point with ω at $\epsilon = 0.05$, 0.1, and 0.2.

semiclassical weights of trajectories over a number of periods of the perturbation is necessary. Instead, here we estimate the tunneling probability in a simpler way, where the weight of the critical trajectory starting at the critical point t_{Ic} on W_s is estimated with the Melnikov method [16,17,23].

The weight of SUMGT trajectories is evaluated from the classical action (6). Actually, if the contribution of the amplitude factor $\sqrt{\frac{\partial^2 S_\Omega}{\partial E_I \partial Q_O}}$ in Eq. (5) is ignored, the tunneling probability of SUMGT is estimated as

$$W_{\mathrm{SUMGT}} \sim \frac{1}{2\pi\hbar} \exp\left\{ -\frac{2}{\hbar} \mathrm{Im} S_\Omega \right\}. \tag{27}$$

The classical action S_Ω for SUMGT trajectories is well approximated by that of the critical trajectory starting at the critical point t_{Ic}, which is also evaluated by using the Melnikov method. The classical action S_Ω is rewritten as

$$S_\Omega(Q_O, t_O, Q_I, E_I) = \int_{t_{Ic}}^{t_O} (H - 2V) dt + E_I(t_O - t_{Ic}), \tag{28}$$

where $V(Q, \omega t) = a(t) V_0(Q)$ and $a(t) = 1 + \epsilon \sin \omega t$. The integration path is taken as $t_{Ic} \to t'_O \to t_O$ ($\mathrm{Re} t'_O = t_O$, $\mathrm{Im} t'_O = \mathrm{Im} t_{Ic}$). Replacing the critical trajectory with the unperturbed one $Q_{0c}(t)$ of the time origin t_{0c} determined by Eq. (21) in order to apply the Melnikov method for evaluating H and the integral of V, and taking into account the facts that $H = E_I$ at $t = t_{Ic}$ and that both H and V approach $a(t)$ as $\mathrm{Re} Q$ goes to negative infinity, we get

$$\begin{aligned}
&\mathrm{Im} S_\Omega(Q_O, t_O, Q_I, E_I) \\
&\sim (1 - E_I) \mathrm{Im} t_{Ic} - \frac{\epsilon}{\omega} \mathrm{Im} \cos \omega t_{0c} \\
&+ \mathrm{Im} \int_{t_{0c}}^{t'_O} dt \int_{t'_O}^{t} ds\, \dot{a}(s) (V_0(Q_{0c}(s)) - 1) \\
&+ \mathrm{Im} \int_{t_{Ic}}^{t_{0c}} dt \int_{t_{Ic}}^{t} ds\, \dot{a}(s) V_0(Q_{0c}(s)) \\
&- 2\mathrm{Im} \int_{t_{0c}}^{t'_O} dt\, \epsilon \sin \omega t (V_0(Q_{0c}(t)) - 1) \\
&- 2\mathrm{Im} \int_{t_{Ic}}^{t_{0c}} dt\, \epsilon \sin \omega t\, V_0(Q_{0c}(t))\, dt.
\end{aligned} \tag{29}$$

Thus, the SUMGT weight is obtained by substituting Eq. (29) into Eq. (27). In a low-frequency range ($\omega \ll 1$), the first two terms of the right-hand side in Eq. (29) become dominant and $\mathrm{Im} S_\Omega$ is estimated by

$$\begin{aligned}
\mathrm{Im} S_\Omega &\sim \frac{1 - E_I}{\omega} \cosh^{-1}\left(\frac{1 - E_I}{\epsilon}\right) \\
&\quad - \frac{\epsilon}{\omega} \sinh\left[\cosh^{-1}\left(\frac{1 - E_I}{\epsilon}\right) \right] \qquad (30) \\
&\sim \frac{1 - E_I}{\omega} \log\left(\frac{2(1 - E_I)}{\epsilon}\right) - \frac{1 - E_I}{\omega}, \qquad (31)
\end{aligned}$$

where Eqs. (25) and (26) are made use of in evaluation of Eqs. (30) and (31), respectively. Equation (31) cannot be used for $\epsilon > 2(1 - E_I)/\mathrm{e}$, because it takes a negative value in this range, although Eq. (30) takes a positive value for $\epsilon < 1 - E_I$. Actually, Eq. (31) takes a negative value at $\epsilon = 0.2$, but it takes positive values at $\epsilon = 0.1$ and 0.05. In any case, if $\epsilon < 1 - E_I$, the imaginary part of the classical action $\mathrm{Im} S_\Omega$ diverges as $\propto 1/\omega$ in the limit $\omega \to 0$, and thereby the tunneling probability (27) decreases as $\propto \exp(-C/\omega)$.

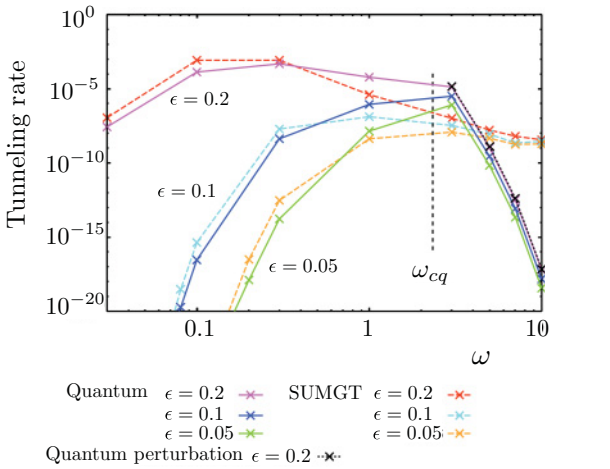

FIG. 6. (Color online) Comparison of quantum tunneling probability with the semiclassical prediction by SUMGT (27) in the frequency range ($0.03 \leqslant \omega \leqslant 10$) at $\epsilon = 0.05, 0.1$, and 0.2. The result of the quantum perturbation (32) is also drawn at $\epsilon = 0.2$ with a thin dotted line.

VI. CHANGE OF TUNNELING PROBABILITY WITH ω

In Fig. 6 the maximum value of the quantum tunneling probability defined by $\max_{-50 \leqslant Q_O \leqslant -30} |\langle Q_O | \hat{\Omega}_1^+(t_O) | P_I \rangle|^2$ is plotted as a function of ω at $\epsilon = 0.05$, 0.1, and 0.2 compared with the semiclassical evaluation W_{SUMGT} given by Eq. (27) with Eq. (29). In this figure, $\omega_{cq} \equiv \frac{1 - E_I}{\hbar}$ is the frequency above which the particle gains a piece of energy enough to go over the potential step by absorbing a single quantum $\hbar\omega$.

In the range $\omega < \omega_{cq}$, W_{SUMGT} well follows the quantum tunneling probability, especially for $\omega < 1$. According to Eq. (27) combined with Eq. (30) or (31), the tunneling probability changes as $\propto \exp(-C/\omega)$ in a low-frequency range, but for the large ϵ, i.e., $\epsilon = 0.2$, it starts to decay in a lower range, namely, for $\omega < 0.1$. The exponential decay of the tunneling probability in the sense of $\propto \exp(-C/\omega)$ as ω goes to zero originates from the divergence of the imaginary depth of the critical point $\mathrm{Im} t_{Ic}$ in the limit of $\omega \to 0$.

Through the whole range of ω, the imaginary depth of the critical point $\mathrm{Im} t_{Ic}$ takes a smaller value for a larger ϵ, resulting in the increase of the tunneling probability with ϵ. According to Eq. (27) combined with Eq. (31), the tunneling probability changes as $\propto \epsilon^{2\omega_{cq}/\omega}$ in the low-frequency range if $\epsilon \ll 1 - E_I$. It turns out that the difference in the tunneling probability between different values of ϵ is enhanced as ω goes to zero.

In the range $\omega > \omega_{cq}$ absorbing a single quantum $\hbar\omega$ makes a particle gain a piece of energy enough to jump over the potential step, that is, $\hbar\omega$ is too large for the semiclassical approximation to be available. Actually, the quantum tunneling probabilities exponentially decrease with increase of ω, while W_{SUMGT} seems to converge on a finite value independent of ϵ. Therefore, SUMGT does not work in this range. In this regime the quantum perturbation method should be available [17].

Practically, the escaping probability due to the absorption of a single quantum $\hbar\omega$ is estimated by a first-order approximation:

$$\lim_{Q_O\to-\infty}|\langle Q_O|\hat{\Omega}_1^+(t_O)|P_I\rangle|^2 \sim \lim_{Q_O\to-\infty}\epsilon^2\pi^2 D_\omega|\langle u_{E_I+\hbar\omega}|V_0|u_{E_I}\rangle|^2, \quad (32)$$

where u_E is a scattering eigenstate of the unperturbed system and the coefficient D_ω is given by the probability amplitude of $u_{E_I+\hbar\omega}$ observed at $Q = Q_O$ [27]:

$$D_\omega = \lim_{Q_O\to-\infty}|\langle Q_O|u_{E_I+\hbar\omega}\rangle|^2 = \frac{1}{2\pi\hbar|P_T|}\times\frac{\sinh^2[\pi(P_R+|P_T|)/\hbar]-\sinh^2[\pi(P_R-|P_T|)/\hbar]}{\sinh^2[\pi(P_R+|P_T|)/\hbar]}, \quad (33)$$

with $P_R=\sqrt{2(E_I+\hbar\omega)}$ and $P_T=-\sqrt{2(E_I+\hbar\omega-1)}$. Hence Eq. (32) indicates the transition probability from u_{E_I} to $u_{E_I+\hbar\omega}$ observed at $Q = Q_O$, and this is nothing more than the so-called "photoassisted" tunneling. Actually the perturbation (thin dotted line in Fig. 6) shows good agreement with the quantum calculation. Since $D_\omega \to \frac{1}{2\pi\hbar|P_T|}$ in the limit $\hbar\omega\to\infty$, the exponential decay is mainly attributed to the transition coefficient $|\langle u_{E_I+\hbar\omega}|V_0|u_{E_I}\rangle|^2$, whose value may depend on the potential shape.

As a result, the quantum tunneling probability is well approximated by SUMGT in the range $\omega<\omega_{cq}$, though it is explained by the photoassisted tunneling absorbing a single quantum $\hbar\omega$ in the range $\omega>\omega_{cq}$. The tunneling probability takes a maximum value in the middle range of ω and decreases exponentially in both limits of $\omega\to 0$ and $\omega\to\infty$. In the case of multidimensional barrier systems [23], the tunneling probability is converged to finite values in both limits of $\omega\to 0$ and $\omega\to\infty$: it is converging to the value estimated by the instanton averaged over the period of the perturbation in the limit of $\omega\to 0$ and is converging to the tunneling rate of the unperturbed system in the limit of $\omega\to\infty$. Namely, the instanton-type tunnelings works in the small and large limits of ω for multidimensional barrier systems. Therefore, the fact that the tunneling probability decays exponentially in the limits of $\omega\to 0$ and $\omega\to\infty$ is a clear evidence that the instanton-type tunneling is substantially prohibited for the periodically perturbed rounded-off step potential.

VII. QUANTUM INTERPRETATION OF NONINSTANTON TUNNELING

A. Model system and quantum solution

In this section we make a quantum interpretation of the tunneling caused by SUMGT. To do this we need a exactly solved model similar in tunneling behavior to the periodically perturbed rounded-off step potential. The model system that satisfies our requirement is a periodically perturbed right-angled step potential whose Hamiltonian is written by

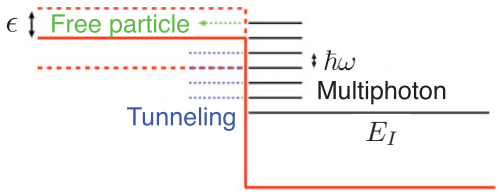

FIG. 7. (Color online) Periodically perturbed right-angled step potential.

$$H(Q,P,\omega t)=\tfrac{1}{2}P^2+(1+\epsilon\sin\omega t)\theta(-Q), \quad (34)$$

where $\theta(x)$ denotes the unit step function.

Let us assume that an input plane wave Ψ_I with an energy E_I is given by

$$\Psi_I(Q)=e^{-\frac{i}{\hbar}E_I t}e^{\frac{i}{\hbar}P_I Q}(P_I=-\sqrt{2E_I}). \quad (35)$$

As shown in Fig. 7, through multiply absorbing or desorbing quanta due to the interaction with the oscillating potential, a reflective wave is formed as a superposition of plane waves with an energy $E_n=E_I+n\hbar\omega$ and a momentum $P_{Rn}=\sqrt{2E_n}$,

$$\Psi_R(Q)=\sum_n R_n e^{-\frac{i}{\hbar}E_n t}e^{\frac{i}{\hbar}P_{Rn}Q}, \quad (36)$$

where R_n is a reflective coefficient. On the other hand, a transmissive wave is obtained as

$$\Psi_T(Q)=\sum_n T_n e^{\frac{i}{\hbar}\frac{\epsilon}{\omega}\cos\omega t}e^{-\frac{i}{\hbar}E_n t}e^{\frac{i}{\hbar}P_{Tn}Q}, \quad (37)$$

where T_n is a transmissive coefficient and $P_{Tn}=-\sqrt{2(E_n-1)}$. The transmissive wave consists of plane waves with a momentum P_{Tn} modulated with the term $e^{\frac{i}{\hbar}\frac{\epsilon}{\omega}\cos\omega t}$ under the effect of the oscillating flat top of the potential [22]. If $E_n<1$, the momentum P_{Tn} takes a negative imaginary value and

$$\lim_{Q\to-\infty}e^{\frac{i}{\hbar}P_{Tn}Q}\to 0. \quad (38)$$

Hence if Q takes a large negative value, the transmissive wave is well approximated by

$$\Psi_T(Q)\sim\sum_{n\geq n^*}T_n e^{\frac{i}{\hbar}\frac{\epsilon}{\omega}\cos\omega t}e^{-\frac{i}{\hbar}E_n t}e^{\frac{i}{\hbar}P_{Tn}Q}, \quad (39)$$

where $n^*=\min\{n|E_n>1\}$.

Reflective and transmissive coefficients, R_n and T_n, are determined with the continuity at the boundary ($Q=0$). The continuity of the wave function, i.e., $\Psi_I+\Psi_R=\Psi_T$, is written as

$$1+\sum_n R_n e^{-in\omega t}=\sum_n T_n e^{\frac{i}{\hbar}\frac{\epsilon}{\omega}\cos\omega t}e^{-in\omega t}. \quad (40)$$

It is also continuously differentiable at $Q=0$, i.e., $\frac{\partial}{\partial Q}\Psi_I+\frac{\partial}{\partial Q}\Psi_R=\frac{\partial}{\partial Q}\Psi_T$:

$$P_I+\sum_n R_n P_{Rn}e^{-in\omega t}=\sum_n T_n P_{Tn}e^{\frac{i}{\hbar}\frac{\epsilon}{\omega}\cos\omega t}e^{-in\omega t}, \quad (41)$$

where $-P_I=P_{R0}$.

Making use of the equality

$$e^{\frac{i}{\hbar}\frac{\epsilon}{\omega}\cos\theta} = \sum_n i^n J_n\left(\frac{\epsilon}{\hbar\omega}\right) e^{in\theta}, \tag{42}$$

where $J_n(z)$ is the Bessel function of the first kind, Eqs. (40) and (41) are respectively reduced to

$$\delta_{n,0} + R_n = \sum_{n'} T_{n'} i^{n'-n} J_{n'-n}\left(\frac{\epsilon}{\hbar\omega}\right) \tag{43}$$

and

$$-\delta_{n,0} P_{Rn} + R_n P_{Rn} = \sum_{n'} T_{n'} P_{Tn'} i^{n'-n} J_{n'-n}\left(\frac{\epsilon}{\hbar\omega}\right). \tag{44}$$

Combining Eqs. (43) and (44) provides a system of linear equations in $\{T_n\}$:

$$\sum_{n'} T_{n'}(P_{Rn} - P_{Tn'}) i^{n'-n} J_{n'-n}\left(\frac{\epsilon}{\hbar\omega}\right) = 2P_{Rn}\delta_{n,0}. \tag{45}$$

B. Scattering eigenstate and evaluation of tunneling probability

By numerically solving Eq. (45), we get $\{T_n\}$ in a physically important energy range and substituting the resultant $\{T_n\}$ into Eq. (43) provides $\{R_n\}$. Figure 8 shows scattering eigenstates reproduced with $\{R_n\}$ and $\{T_n\}$ numerically obtained at $\omega = 0.3$ for the cases $\epsilon = 0$, 0.05, 0.1, and 0.2. The wave forms in Fig. 8 are very similar to those of the rounded-off step potential in Fig. 1. Actually, the tunneling tail of the unperturbed system at $\epsilon = 0$ drops off exponentially in the potential wall. The tunneling wave of the perturbed system forms an almost flat probability in the transmissive side ($Q < 0$) and it increases with ϵ.

Figure 9 shows the transmissive weights $|T_n|^2$ at $\epsilon = 0.05$, 0.1, and 0.2 as a function of energy E. The weight $|T_n|^2$ at each strength of the perturbation forms a plateau with its center at $E = E_I$ and with a width of 2ϵ. However, the transmissive components in Eq. (37) with a large T_n on the flat top of this plateau do not actually contribute to tunneling, because the energy range of the flat top is

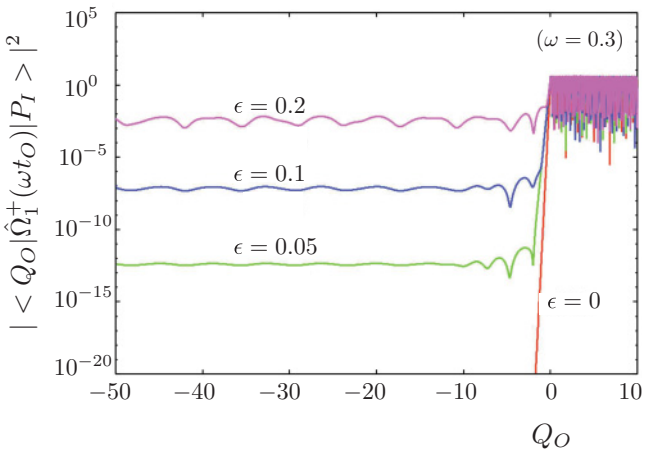

FIG. 8. (Color online) Probabilistic amplitudes of scattering eigenstates for the right-angled step potential at $\epsilon = 0$, 0.05, 0.1, and 0.2. The parameters take the same values as those of the rounded-off step in Fig. 1.

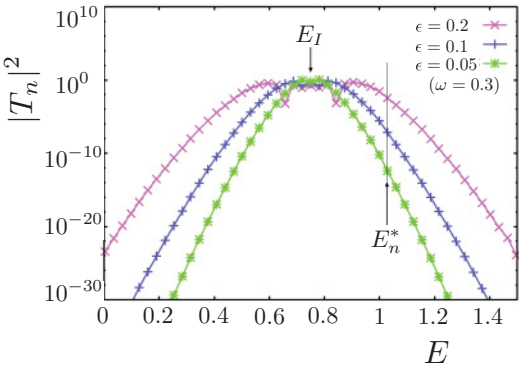

FIG. 9. (Color online) Transmissive weights $|T_n|^2$ as a function of energy at $\epsilon = 0.05$, 0.1, 0.2, and at $\omega = 0.3$.

less than the potential height at rest, i.e., $E_n \leqslant E_I + \epsilon < 1$, and the tunneling probability mainly determined by $e^{\frac{i}{\hbar}P_{Tn}Q}$ exponentially decays like instanton in the limit $Q \to -\infty$, as shown in Eq. (38). It is natural to consider that the transmissive components on the flat top are the components which can be approximated with the perturbation based on the instanton method. This is the quantum interpretation of the substantial prohibition of the instanton-type tunneling.

The transmissive components for $n \geqslant n^*$ really contribute to tunneling and the component of $n = n^*$ makes the dominant contribution, because from Eq. (39) the contribution of each component is mainly determined by $|T_n|^2$, and $|T_{n^*}|^2$ takes the largest value among $|T_n|^2$'s for $n \geqslant n^*$ (see Fig. 9). Indeed, $|T_{n^*}|^2$ at each strength of perturbation almost coincides with the corresponding tunneling probability in Fig. 8. The fact that the plateau changes in shape with ϵ, especially in the slope of its upper cliff, well explains the change of tunneling probability. The classical trajectory corresponding to the transmissive component at $n = n^*$ has the smallest negative real momentum P_{Tn^*} among P_{Tn}'s for $n \geqslant n^*$ and must play the same role of SUMGT trajectories, although due to lack of the separatrix W_s there is no critical trajectory guiding it as the case of the rounded-off step.

To explore the properties of the transmissive coefficients $\{T_n\}$, we develop an approximation method. The system of linear equations in $\{T_n\}$ (45) includes the Bessel functions $\{J_n(\frac{\epsilon}{\hbar\omega})\}$ in coefficients of $\{T_n\}$ and the coefficients of $\{T_n\}$ substantially form a band matrix, because $J_n(\frac{\epsilon}{\hbar\omega})$ takes a large value only in the range $(|n| < \frac{\epsilon}{\hbar\omega})$. Let us make a plausible assumption that $T_n \sim O[J_n(\frac{\epsilon}{\hbar\omega})]$, though we do not have any mathematical proof, and we estimate the order of T_n by using the asymptotic expansions of J_n.

In the range $\hbar\omega \ll \epsilon$, if $n \ll \frac{\epsilon}{\hbar\omega}$, $|T_n|^2$ is roughly estimated as a constant value:

$$|T_n|^2 \sim \left|J_n\left(\frac{\epsilon}{\hbar\omega}\right)\right|^2 \sim \frac{2\hbar\omega}{\pi\epsilon}, \tag{46}$$

which corresponds the flat top of the plateau in the range $(E_I - \epsilon < E < E_I + \epsilon)$ in Fig. 9. For $n \gg \frac{\epsilon}{\hbar\omega}$, the estimation becomes

$$|T_n|^2 \sim \left|J_n\left(\frac{\epsilon}{\hbar\omega}\right)\right|^2 \sim \frac{1}{2\pi n}\exp\left(-2n\left[\log\left(\frac{2n\hbar\omega}{\epsilon}\right) - 1\right]\right). \tag{47}$$

If $n > \frac{e}{2}\frac{\epsilon}{\hbar\omega} > \frac{\epsilon}{\hbar\omega}$, then $\log(\frac{2n\hbar\omega}{\epsilon}) - 1 > 0$, and Eq. (47) indicates that $|T_n|^2$ decays with n more than exponentially. For $\frac{e}{2}\frac{\epsilon}{\hbar\omega} \geqslant n > \frac{\epsilon}{\hbar\omega}$, this approximation is not available, though the numerical calculation shows that $|T_n|^2$ decays exponentially even in this range.

In the case that $n^* > \frac{e}{2}\frac{\epsilon}{\hbar\omega}$, the approximate tunneling probability W_T is defined by

$$
\begin{aligned}
|T_{n^*}|^2 &\sim \left| J_{n^*}\left(\frac{\epsilon}{\hbar\omega}\right)\right|^2 \\
&\sim \frac{1}{2\pi n^*}\exp\left(-2n^*\left[\log\left(\frac{2n^*\hbar\omega}{\epsilon}\right)-1\right]\right) \\
&\sim \frac{\omega}{2\omega_{cq}}\exp\left(-2\frac{\omega_{cq}}{\omega}\left[\log\left(\frac{2(1-E_I)}{\epsilon}\right)-1\right]\right) \\
&\equiv W_T, \qquad (48)
\end{aligned}
$$

where $\omega_{cq} \equiv \frac{1-E_I}{\hbar}$ and the approximation $n^*\hbar\omega \sim 1 - E_I$ is used. The probability W_T is as same as the tunneling probability W_{SUMGT}, approximated by Eq. (27) and combined with Eq. (31), except for the prefactor. Then it is expected that as ω goes to zero W_T decreases exponentially but more rapidly than W_{SUMGT} by the prefactor $\frac{\omega}{2\omega_{cq}}$. On the other hand, it increases as $\propto \epsilon^{2\omega_{cq}/\omega}$ with ϵ, which is the same as that for W_{SUMGT} if $\epsilon \ll 1 - E_I$. Note that W_T does not make a correct estimation for $\epsilon > 2(1 - E_I)/e$, because the exponential function in W_T takes a value more than unity.

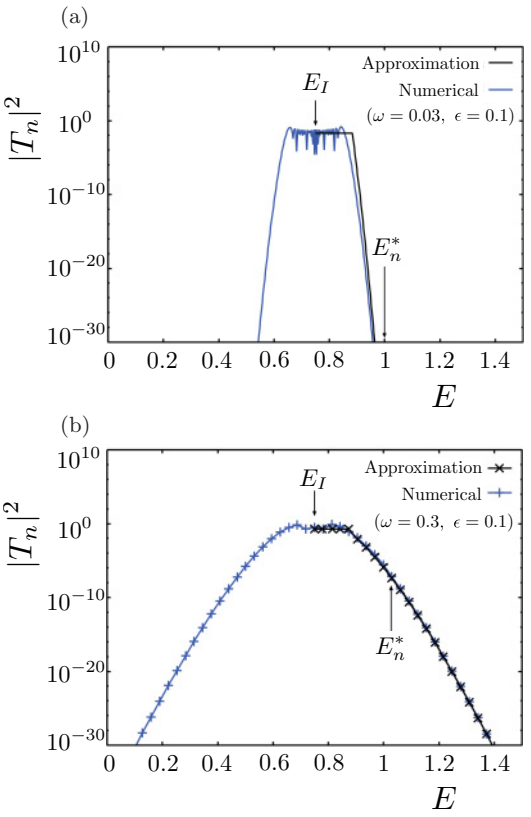

FIG. 10. (Color online) Comparison of $|T_n|^2$ with the approximation given by Eq. (46) for $0 \leqslant n \leqslant \frac{e}{2}\frac{\epsilon}{\hbar\omega}$ and Eq. (47) for $n > \frac{e}{2}\frac{\epsilon}{\hbar\omega}$ at $\epsilon = 0.1$: (a) $\omega = 0.03$ and (b) $\omega = 0.3$.

Actually, it cannot be applied for $\epsilon = 0.2$, although it works for $\epsilon = 0.1$ and 0.05.

In Fig. 10, $|T_n|^2$ numerically obtained as a function of energy E is compared with the approximation gathering Eqs. (46) and (47) at $\epsilon = 0.1$ for two values of ω, $\omega = 0.03$ and 0.3. The height of the plateau formed by $|T_n|^2$ is well approximated by Eq. (46) for both values of ω. Equation (47) almost coincides with $|T_n|^2$ in the cliff at $\omega = 0.3$ but slightly overestimates it at $\omega = 0.03$. Since the cliff becomes steeper exponentially with decrease of ω, the tunneling probability approximated by $|T_n|^2$ at $n = n^*$, i.e., $|T_{n^*}|^2 \sim W_T$, decays exponentially with decrease of ω. As shown in Fig. 10(a), $|T_{n^*}|^2$ at $\omega = 0.03$ is so small that it is out of our numerical precision.

In the range $\omega > \omega_{cq}$, $n^* = 1$, and so taking into account only T_0 and T_1 in Eq. (45) and making use of the approximation $J_{-1}(\frac{\epsilon}{\hbar\omega}) \sim -\frac{\epsilon}{\hbar\omega}$ give

$$
|T_1|^2 \sim \left(\frac{\epsilon}{\hbar\omega}\right)^2\left|\frac{p_I(p_{R1}-p_{T0})}{(p_I+p_{T0})(p_{R1}-p_{T1})}\right|^2 < \left(\frac{\epsilon}{2\hbar\omega}\right)^2. \qquad (49)
$$

Note that the same estimation is obtained for a periodically perturbed box potential [22]. The tunneling probability decays as $\propto \frac{1}{\omega^2}$ in the limit $\omega \to \infty$, which is different from the case of the rounded-off step for which the tunneling probability dumps exponentially. As discussed later, the difference in the decay comes from the difference in the potential shapes.

C. Energy spectrum

In the same way as Eq. (4), the energy spectrum of the tunneling wave is defined by

$$
|\tilde{\Psi}(E)|^2 = \left|\frac{1}{2\pi\hbar}\int_{-\infty}^{\infty}\Psi_T(Q)e^{\frac{i}{\hbar}Et}dt\right|^2. \qquad (50)
$$

Figure 11 shows energy spectra at $\epsilon = 0.05$, 0.1, and 0.2. As in the case of the rounded-off step, each spectrum forms a plateau whose height increases with ϵ and whose flat top width is nearly equal to 2ϵ.

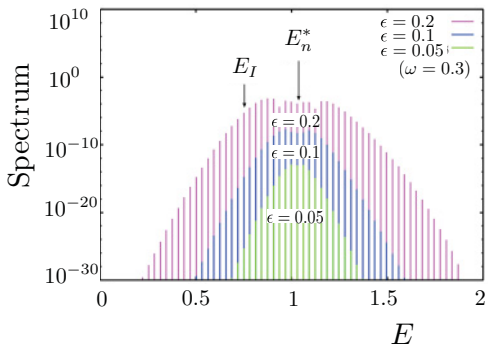

FIG. 11. (Color online) Tunneling energy spectra calculated by Eq. (50) at $\epsilon = 0.05$, 0.1, and 0.2.

From Eq. (39), $|\tilde{\Psi}(E)|$ is approximated with the component at $n = n^*$:

$$
\begin{aligned}
|\tilde{\Psi}(E)| &\sim \left| \frac{1}{2\pi\hbar} \int_{-\infty}^{\infty} dt e^{\frac{i}{\hbar}Et} \sum_{n \geqslant n^*} T_n e^{\frac{i}{\hbar}\frac{\epsilon}{\omega}\cos\omega t} e^{-\frac{i}{\hbar}E_n t} e^{\frac{i}{\hbar}P_{Tn}Q} \right| \\
&= \left| \frac{1}{2\pi\hbar} \sum_{n \geqslant n^*} T_n e^{\frac{i}{\hbar}P_{Tn}Q} \sum_m i^m J_m\left(\frac{\epsilon}{\hbar\omega}\right) \right. \\
&\quad \left. \times \int_{-\infty}^{\infty} dt e^{im\omega t} e^{\frac{i}{\hbar}Et} e^{-\frac{i}{\hbar}E_n t} \right| \\
&\sim |T_{n^*}| \sum_m \left| J_m\left(\frac{\epsilon}{\hbar\omega}\right) \right| \delta(E - E_{n^*} + m\hbar\omega), \qquad (51)
\end{aligned}
$$

where the equality (42) is used. Then the normalized tunneling energy spectrum is obtained as

$$
|\tilde{\Psi}(E)|^2 \sim |T_{n^*}|^2 \sum_m \left| J_m\left(\frac{\epsilon}{\hbar\omega}\right) \right|^2 \delta_{E, E_{n^*} + m\hbar\omega}, \qquad (52)
$$

where it is normalized as $\delta(E - E_n)^2 \to \delta_{E,E_n}$. The term $e^{\frac{i}{\hbar}\frac{\epsilon}{\omega}\cos\omega t}$ in the first right-hand side of Eq. (51) is attributed to the periodicity of the perturbation and creates through equality (42) a discrete spectrum whose envelope forms a plateau. Indeed, applying the approximations used in Eqs. (46) and (47) to $|J_m(\frac{\epsilon}{\hbar\omega})|^2$ in Eq. (52) provides the tunneling energy spectrum, forming a plateau as shown in Fig. 12. The approximate plateau spectrum at $\epsilon = 0.1$ shows good agreement with the numerical result in Fig. 11. Since the same approximation in Eqs. (46) and (47) is valid for both $|T_n|^2$ and $|\tilde{\Psi}(E)|^2$, the tunneling plateau spectra numerically obtained in Fig. 11 are very similar in shape to numerically obtained $|T_n|^2$'s in Fig. 9, although their heights and centers are different between $|T_n|^2$ and $|\tilde{\Psi}(E)|^2$.

D. Change of the tunneling probability with ω

Figure 13 shows the change of the tunneling probability defined by $\max_{-50<Q<-20} |\Psi_T(Q)|^2$ with ω for the three cases, $\epsilon = 0.05$, 0.1, and 0.2. In the range $\omega < \omega_{cq}$, the tunneling probability decays exponentially with decrease of ω and is well followed by the approximate tunneling probability W_T defined by Eq. (48), though it is shown only for the case of $\epsilon = 0.1$. As

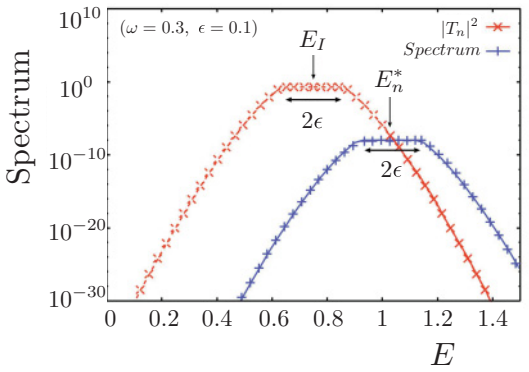

FIG. 12. (Color online) The tunneling energy spectrum obtained by Eq. (52) with the approximations in Eqs. (46) and (47) at $\omega = 0.3$ and $\epsilon = 0.1$. For comparison, the approximate $|T_n|^2$ obtained by Eqs. (46) and (47) is also drawn.

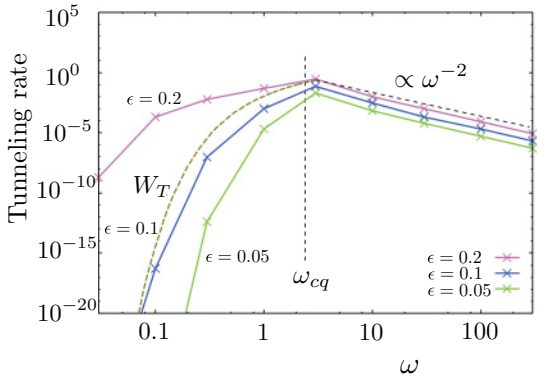

FIG. 13. (Color online) Change of the tunneling probability with ω. The three cases at $\epsilon = 0.05$, 0.1, and 0.2 are drawn. The approximate tunneling probability W_T defined by Eq. (48) is also drawn at $\epsilon = 0.1$.

a result, the changes of the tunneling probability for the three representative values of ϵ are very similar to those for the rounded-off step in Fig. 6. However, the tunneling probability of the right-angled step always takes a larger value than that of the rounded-off step near ω_{cq}, for example, $\omega = 1$.

For $\epsilon = 0.05$ and 0.1, the tunneling probability of the right-angled step decays more steeply as ω goes to zero than that of the rounded-off potential. This may be due to the effect of the prefactor $\frac{\omega}{2\omega_{cq}}$ in Eq. (48). On the other hand, for $\epsilon = 0.2$ the tunneling probability of the rounded-off step becomes larger in a lower range of ω than that of the right-angled step and takes the maximum value around $\omega = 0.3$, though the tunneling probability of the right-angled step has no maximum below ω_{cq}. This difference possibly comes from the difference in the potential shapes. Figure 14 shows results for the rounded-off step with a sharper potential edge:

$$
V_S(Q,t) = (1 + \epsilon \sin\omega t) \frac{1}{1 + e^{Q/w_d}}, \quad (w_d = 0.5). \qquad (53)
$$

As shown in Fig. 14, the tunneling probability of this potential does not take a maximum value for $\omega < \omega_{cq}$ and behaves in an intermediate manner between the rounded-off step and the right-angled step. Then it may be expected that the tunneling probability of the potential (53) converges on that of the right-angled step in the limit $w_d \to 0$.

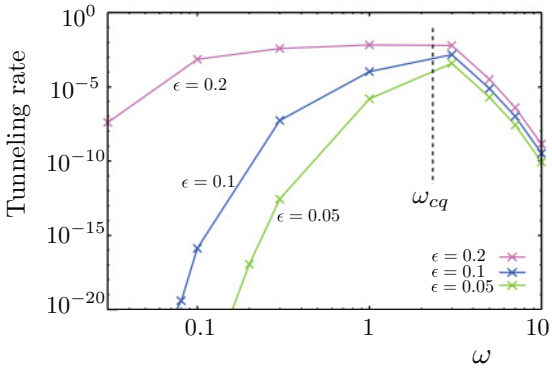

FIG. 14. (Color online) Change of the tunneling probability with ω for the potential (53). The three cases at $\epsilon = 0.05$, 0.1, and 0.2 are drawn.

In the range $\omega > \omega_{cq}$, the tunneling probability takes a maximum value just above ω_{cq} and decays as $\propto \epsilon^2/\omega^2$ with increase of ω, as predicted by Eq. (49). On the other hand, the tunneling probability decreases exponentially with ω for the rounded-off step (see Fig. 6). However, comparing Fig. 14 with Figs. 6 and 13, the tunneling probability of the rounded-off step (53) seems to approach to that of the right-angled step in the limit $w_d \to 0$.

VIII. DISCUSSION

In this paper we have investigated the noninstanton tunneling, for which the instanton-type tunneling makes an infinitesimal contribution while the stable-unstable manifold-guided tunneling (SUMGT) dominates the tunneling process in the semiclassical regime instead [23].

First we have studied the change of the tunneling probability with the perturbation frequency ω taking the periodically perturbed rounded-off step potential as a model system [23]. In the range $\omega < \omega_{cq} (\equiv (1 - E_I)/\hbar\omega)$, namely, the semiclassical regime, the change of the tunneling probability with ω is well explained by SUMGT with the help of the Melnikov method. The imaginary depth of the critical point, i.e., the intersection between the complex stable manifold and the initial plane, mainly determines the tunneling probability. The imaginary depth of the critical point $\mathrm{Im}t_{Ic}$ diverges as $\propto 1/\omega$ in the limit $\omega \to 0$. It turns out that the imaginary part of the classical action $\mathrm{Im}S_\Omega$ also diverges as $\propto 1/\omega$ in the limit $\omega \to 0$, thereby decreasing the tunneling probability exponentially in the sense of $\propto \exp(-C/\omega)$. Therefore the exponential decay of the tunneling probability in the limit $\omega \to 0$ is the characteristic of the tunneling governed by SUMGT. In the case that the instanton-type tunneling makes a finite contribution, e.g., the multidimensional barrier tunneling, it takes the place of SUMGT in the limit $\omega \to 0$ and makes a finite tunneling probability predicted by the perturbed instanton method, i.e., averaged instanton weight over the period of the perturbation [17].

In the range $\omega > \omega_{cq}$, the particle gains a piece of energy with the absorption of a single quantum $\hbar\omega$ large enough to go over the potential step. Therefore, this is a non-semiclassical regime, and the lowest order quantum perturbation well approximates the tunneling probability. Actually the transition probability $|\langle u_{E_I+\hbar\omega}|V_0|u_{E_I}\rangle|^2$ in Eq. (32) mainly determines the tunneling probability and well reproduces the exponential decay in the limit $\omega \to \infty$.

Next we have provided the quantum interpretation of the noninstanton tunneling with the exactly solvable model, the periodically perturbed right-angled step potential, for which the tunneling wave is obtained by summing up over n products of transition coefficient T_n and unperturbed scattering eigenstate at $E_n = E_I + n\hbar\omega$ modulated by the periodical perturbation. This model shows a similar change of the tunneling probability with ω in the range $\omega < \omega_{cq}$ to that of the rounded-off step potential. Actually it seems to decay exponentially as $\propto \omega \exp(-C/\omega)$ when ω goes to zero, as the rounded-off potential does except for the prefactor ω. On the other hand, it shows a power-law decay as $\propto 1/\omega^2$ in the range $\omega > \omega_{cq}$, while the exponential decay is observed for the rounded-off step. Those differences seem to be attributed to the difference in potential shape between the rounded-off and right-angled steps.

In the regime of the instanton-type tunneling, energy exchange with an external force [or other degree(s) of freedom] should occur in the classically arrowed (acceptable) energy range, namely, $(E_I - \epsilon \leqslant E \leqslant E_I + \epsilon)$. The tunneling probability is chiefly determined by the tunneling wave amplitudes of unperturbed (scattering) eigenstates of an energy $E_I + n\hbar\omega$ in this range, because the transition coefficients T_n are in the same order $O(\hbar\omega/\epsilon)$. For a step-shaped potential, the tunneling tail of an unperturbed eigenstate decays exponentially in the potential wall so that the instanton-type tunneling is substantially unobserved.

In the regime of SUMGT, the particle absorbs a huge number quanta $n\hbar\omega$ through the interaction with an external force [or other degree(s) of freedom] and jumps up to the energy range over the potential top in which the classical motion is allowed in the transmissive region. Such a huge energy jump beyond the range $(E_I - \epsilon \leqslant E \leqslant E_I + \epsilon)$ is classically forbidden and the magnitude of transition coefficient T_n becomes exponentially small with increase of n, i.e., with increase of the amount of energy gained in the transition. Since the transmissive wave amplitude of a scattering eigenstate is of $O(1)$ over the potential top, the coefficient of the transition to the state just above potential top, i.e., T_{n^*}, mainly determines the tunneling probability. This quantum process really corresponds to the mechanism of SUMGT, in which the tunneling trajectories undergo huge jumps in energy with the guide of the complex stable manifold. The exponential decay of the tunneling probability as ω goes to zero is due to the exponential decay of T_{n^*}, while this is explained in SUMGT by the increase of the imaginary depth of the critical point resulting in the increase of the imaginary part of the classical action. Usually it is not easy to estimate the transmissive coefficient of the huge jump caused by the multiple absorption of quanta for any shaped potential by using a quantum perturbation theory, especially in the limit of $\omega \to 0$. Instead SUMGT combined with the Melnikov method gives an appropriate semiclassical interpretation to understand the tunneling process and provides a practical method to estimate the tunneling probability, if the potential under consideration is analytic.

For periodically perturbed (or multidimensional) barrier potentials of a relatively thin wall the competition between SUMGT and instanton-type tunneling is observed. The winner which dominates the tunneling process is determined by the comparison of the imaginary depths between the instanton trajectory and the critical point, i.e., the imaginary depth of SUMGT trajectories. Indeed, the one nearer to the real space is the winner. It is very interesting to interpret the competition between SUMGT and instanton from the viewpoint of a quantum process, i.e., a competition between quantum barrier penetration and quantum transition to the classically acceptable energy range with the multiple absorption of quanta. A periodically perturbed box potential may be a good model for this research, but we postpone it for a future publication.

ACKNOWLEDGMENTS

This work was supported by a Grant-in-Aid for Scientific Research (B), No. 20340100, from JSPA.

[1] *Tunneling in Complex Systems*, edited by S. Tomsovic (World Scientific, Singapore, 1998).

[2] J. Ankerhold, *Quantum Tunneling in Complex Systems, The Semiclassical Approach* (Springer-Verlag, Berlin-Heidelberg, 2007).

[3] S. Keshavamurthy, Int. Rev. Phys. Chem. **26**, 521 (2007).

[4] *Dynamical Tunneling: Theory and Experiment*, edited by S. Keshavamurthy and P. Schlagheck (CRC Press, Taylor & Francis Group, 2011).

[5] O. Bohigas, S. Tomsovic, and D. Ullmo, Phys. Rev. Lett. **65**, 5 (1990); Phys. Rep. **223**, 43 (1993).

[6] S. C. Creagh and N. D. Whelan, Phys. Rev. Lett. **84**, 4084 (2000).

[7] S. C. Creagh, Nonlinearity **17**, 1261 (2004); **18**, 2089 (2005); C. S. Drew, S. C. Creagh, and R. H. Tew, Phys. Rev. A **72**, 062501 (2005).

[8] W. K. Hensinger *et al.*, Nature **412**, 52 (2001); D. A. Steck, W. H. Oskay, and M. G. Raizen, Science **293**, 274 (2001); C. Dembowski, H.-D. Gräf, A. Heine, R. Hofferbert, H. Rehfeld, and A. Richter, Phys. Rev. Lett. **84**, 867 (2000).

[9] O. Brodier, P. Schlagheck, and D. Ullmo, Phys. Rev. Lett. **87**, 064101 (2001); Ann. Phys. (N.Y.) **300**, 88 (2002); C. Eltschka and P. Schlagheck, Phys. Rev. Lett. **94**, 014101 (2005).

[10] A. Bäcker, R. Ketzmerick, S. Löck, and L. Schilling, Phys. Rev. Lett. **100**, 104101 (2008); A. Bäcker, R. Ketzmerick, S. Löck, M. Robnik, G. Vidmar, R. Hohmann, U. Kuhl, and H. J. Stockmann, *ibid.* **100**, 174103 (2008); A. Bäcker, R. Ketzmerick, S. Löck, J. Wiersig, and M. Hentschel, Phys. Rev. A **79**, 063804 (2009); S. Löck, A. Bäcker, R. Ketzmerick, and P. Schlagheck, Rhys. Rev. Lett. **104**, 114101 (2010).

[11] A. Shudo and K. S. Ikeda, Phys. Rev. Lett. **74**, 682 (1995); Physica D **115**, 234 (1998); T. Onishi, A. Shudo, K. S. Ikeda, and K. Takahashi, Phys. Rev. E **64**, 025201(R) (2001); **68**, 056211 (2003).

[12] A. Shudo, Y. Ishii, and K. S. Ikeda, J. Phys. A **35**, L225 (2002); Europhys. Lett. **81**, 50003 (2008); J. Phys. A **42**, 265101 (2009); **42**, 265102 (2009).

[13] L. S. Schulman, *Techniques and Applications of Path Integration* (Wiley, New York, 1981).

[14] K. Takahashi, A. Yoshimoto, and K. S. Ikeda, Phys. Lett. A **297**, 370 (2002); K. Takahashi and K. S. Ikeda, J. Phys. A **36**, 7953 (2003).

[15] K. Takahashi and K. S. Ikeda, Europhys. Lett. **71**, 193 (2005); J. Phys. A **41**, 095101 (2008).

[16] K. Takahashi and K. S. Ikeda, Phys. Rev. A **79**, 052114 (2009).

[17] K. Takahashi and K. S. Ikeda, J. Phys. A **43**, 192001 (2010).

[18] F. Bezrukov and D. Levkov, J. Exp. Theor. Phys. **98**, 820 (2004); D. G. Levkov, A. G. Panin, and S. M. Sibiryakov, Phys. Rev. Lett. **99**, 170407 (2007); Phys. Rev. E **76**, 046209 (2007); J. Phys. A **42**, 205102 (2009).

[19] W. H. Miller, J. Chem. Phys. **53**, 1949 (1970); Adv. Chem. Phys. **25**, 69 (1974).

[20] The Julia set is the boundary of the bounded set of a complex map. If the complex map $F(q,p)$ is given in the complex phase space (q,p), the forward and backward Julia sets are respectively defined by $J^{\pm} = \partial^{\pm} K$, where $K^{\pm} = \{(p,q) \in \mathbf{C}^2 F^n(q,p)$ is bounded by $(n \to \pm\infty)\}$. The complex stable and unstable manifolds are dense in forward and backward Julia sets [21].

[21] E. Bedford and J. Smillie, J. Am. Math. Soc. **4**, 657 (1991).

[22] M. Büttiker and R. Landauer, Phys. Rev. Lett. **49**, 1739 (1982); Phys. Scr. **32**, 429 (1985).

[23] K. Takahashi and K. S. Ikeda, Phys. Rev. Lett. **97**, 240403 (2006).

[24] K. Takahashi and K. S. Ikeda, Ann. Phys. (N.Y.) **283**, 94 (2000).

[25] V. K. Melnikov, Trans. Mosc. Math. Soc. **12**, 1 (1963).

[26] S. Wiggins, *Introduction to Applied Nonlinear Dynamical Systems and Chaos* (Springer-Verlag, New York, 1990).

[27] L. D. Landau and E. M. Lifshitz, *Quantum Mechanics Non-relativistic Theory* (Butterworth Heinemann, Amsterdam, 1977).